JBC Papers in Press. Published on November 28, 2011 as Manuscript M111.305938
The latest version is at http://www.jbc.org/cgi/doi/10.1074/jbc.M111.305938

# Torque generation and utilization in the motor enzyme $F_oF_1$-ATP synthase: half-torque $F_1$ with short-sized pushrod helix and reduced ATP synthesis by half-torque $F_oF_1$.

Eiji Usukura[1], Toshiharu Suzuki[2], Shou Furuike[3], Naoki Soga[4], Ei-ichiro Saita[2], Toru Hisabori[1,2], Kazuhiko Kinosita, Jr.[4] and Masasuke Yoshida[2,5]

[1]Chemical Resources Laboratory, Tokyo institute of technology, Nagatsuta 4259, Yokohama 226-8503. [2]ICORP ATP-Synthesis Regulation Project, Japan Science and Technology Agency (JST), 2-3-6 Aomi, Tokyo 135-0064. [3] Department of Physics, Osaka Medical College, Takatsuki, Osaka 569-8686. [4]Department of Physics, Waseda University, Shinjuku, Tokyo 171-0033. [5] Department of Molecular Bioscience, Kyoto Sangyo University, Kamigamo-Motoyama, Kyoto 603-8555, Japan

Running title: $F_oF_1$-ATP synthase with half-torque $F_1$

Address correspondence to: Masasuke Yoshida, Department of Molecular Bioscience, Kyoto Sangyo University, Kamigamo-Motoyama, Kyoto 603-8555, Japan, Tel.: (+81) 75-705-2962; masasuke.yoshida@cc.kyoto-su.ac.jp

Keywords: ATP synthase, $F_1$, motor, torque

**Background:** ATP synthase ($F_oF_1$) is a rotary motor enzyme.
**Results:** $F_1$ with a short-sized helix-1 in β subunit rotates with half the normal torque and supports reduced ATP synthesis activity.
**Conclusion:** Helix-1 acts as a "pushrod" to generate torque and torque-reduced $F_oF_1$ retains catalytic ability of ATP synthesis.
**Significance**: Generation and utilization of the torque are crucial for motor enzymes.

## SUMMARY

**ATP synthase ($F_oF_1$) is made of two motors, a proton-driven motor ($F_o$) and an ATP-driven motor ($F_1$), connected by a common rotary shaft, and catalyzes proton flow-driven ATP synthesis and ATP-driven proton pumping. In $F_1$, the central γ subunit rotates inside the $\alpha_3\beta_3$-ring. Here we report structural features of $F_1$ responsible for torque generation and catalytic ability of the low-torque $F_oF_1$. (i) Deletion of one or two turns in the α-helix in the C-terminal domain of catalytic β subunit at the rotor/stator contact region generates mutant $F_1$s, termed $F_{1(1/2)}$s, that rotate with about half the normal torque. This helix would support the helix-loop-helix structure acting as a solid "pushrod" to push the rotor γ subunit, but the short helix in $F_{1(1/2)}$s would fail to accomplish this task. (ii) Three different half-torque $F_oF_{1(1/2)}$s were purified and reconstituted into proteoliposomes. They carry out ATP-driven proton-pumping and build up the same small transmembrane ΔpH, indicating that the final ΔpH is directly related to the amount of torque. (iii) The half-torque $F_oF_{1(1/2)}$s can catalyze ATP synthesis, though slowly. The rate of synthesis varies widely among the three $F_oF_{1(1/2)}$s, which suggests that the rate reflects subtle conformational variations of individual mutants.**

$F_oF_1$-ATP synthase ($F_oF_1$) catalyzes synthesis of ATP in mitochondria, chloroplasts, and bacteria in oxidative- and photo-phosphorylation, using the energy of proton translocation caused by the proton motive force across membranes (pmf)[1]. Proton

translocation through membrane-embedded $F_o$ portion drives ATP synthesis in membrane-protruding $F_1$ portion and, in the reverse reaction, ATP hydrolysis in $F_1$ can drive pumping back protons through $F_o$. These two reactions, the inward/outward proton translocation in $F_o$ and synthesis/hydrolysis in $F_1$, are coupled by mechanical rotation (1-10). Both $F_o$ and $F_1$ are rotary motors; $F_o$-motor is driven by downhill proton translocation and $F_1$-motor by ATP hydrolysis, and the two motors share a common rotary shaft. When pmf is high, $F_o$ drives rotation of the shaft that results in ATP synthesis in $F_1$. When chemical potential of ATP hydrolysis exceeds pmf, $F_1$ rotates the shaft and $F_o$ is forced to pump protons. Indeed, isolated $F_1$ rotates when it hydrolyzes ATP (11) and the reverse rotation by an external force results in ATP synthesis (12,13).

ATP-driven rotation of the isolated $F_1$ has been extensively studied by using a minimum motor complex consisting of $\alpha_3\beta_3\gamma$ subunits from thermophilic *Bacillus* PS3 (14-16), which we also refer to as $F_1$ in this paper unless otherwise indicated. The γ subunit is a rotor subunit. Its N- and C-terminal helices form a coiled coil and are deeply inserted into the cavity of the stator $\alpha_3\beta_3$-ring. The globular domain of γ subunit resides outside of the cavity of the $\alpha_3\beta_3$-ring (Fig. 1, left panel). To visualize rotation, the $\alpha_3\beta_3$-ring is immobilized on the glass surface and a bead (or bead duplex) is attached to the globular domain of γ subunit. A single cycle rotates the γ subunit 120° consuming one ATP, meaning $F_1$ carries out three reaction cycles per revolution. The 120° cycle begins with a pause at 0°, then a ~80°-step rotation is followed by another pause, and lastly a ~40°-step rotation occurs. $F_1$ waits for a substrate ATP during the pause at 0° ("ATP-waiting dwell") and rotates ~80° upon ATP binding. A pause at ~80° ("catalytic dwell") is ~2 ms, independent of ATP concentration, representing the period required for hydrolytic cleavage of ATP and release of $P_i$ from the catalytic site.

The torque of ATP-driven $F_1$-motor estimated from rotation speed, bead radius, rotation radius, and viscosity of aqueous medium amounts to ~40 pN·nm (17). The energy required for a 120° rotation (~40 pN·nm x $2\pi/3$ radian) is roughly equal to the free energy liberated from hydrolysis of an ATP molecule (~90 pN·nm) under physiological conditions and, therefore, energy conversion by $F_1$-motor is very efficient. The torque of $F_1$ is generated from sequential interactions between a rotor γ subunit and three catalytic β subunits in the stator $\alpha_3\beta_3$-ring (18). According to the crystal structures (19,20), β subunits can interact directly with the γ subunit at the two positions, the "sleeve" and the "orifice" regions (Fig 1, left panel). A mutant $F_1$, whose γ subunit is truncated at the C-terminus and loses interactions with $\alpha_3\beta_3$-ring at the sleeve region, rotates with half the normal torque (21). Inversely, $F_1$ devoid of the entire N-terminal helix, which preserves the sleeve interactions but loses many interactions at the orifice, also rotates with half the normal torque (22). Therefore, the orifice interactions alone can produce half of the total torque, and the sleeve interactions, probably with the assistance of some of the orifice interactions, produce another half.

At the orifice region, the helix-1−loop−helix-2 structure in C-terminal domain of β subunit makes contact with the γ subunit (19). The loop in the structure contains a well-conserved, DELSDEAD acidic cluster sequence, but its acidic nature is not essential for torque generation (23). Recently, it was shown that deletion of three or four residues in the loop does not impair ATP synthesis activity of $F_oF_1$ (24). If neither acidic residues in the loop nor the full-length loop itself are essential for rotation, what structural features of the orifice region are responsible for torque generation? Here, we report isolation of mutant $F_1$s that exert half the normal torque, indicating that the full-length helix-1 acts as a "pushrod" for the γ subunit to generate half of the total torque. Then, we addressed the next question; if the $F_1$ portion of

$F_oF_1$ wastes a large fraction of the energy transferred from the $F_o$-motor, can it synthesize ATP? The results show that it can, though slowly.

## EXPERIMENTAL PROCEDURES

*Strains, plasmids, and proteins* ---- *Escherichia coli* strain JM109 was used for the genetic manipulation and JM103 (ΔuncB-uncD), which does not express *E. coli* $F_oF_1$, for the expression of $F_1$ and $F_oF_1$ from thermophilic *Bacillus* PS3. Mutations of *Bacillus* PS3 $F_1$ were introduced into the plasmid pKAGB1/HC95 which expresses the $\alpha(C193S)_3\beta$(10-histidine tag at N terminus)$_3\gamma$(S107C/I210C) complex of $F_1$. Wild-type and mutant $F_1$ were expressed and purified as described (25) except for two procedures. Heat treatment to precipitate heat-labile *E. coli* proteins was carried out at 64°C for 20 min for wild-type $F_1$ but at 60°C for 10 min for the mutants. The procedure to remove endogenously bound nucleotides was omitted for the mutants because mutants without bound nucleotides tend to dissociate. The purified $F_1$ was stored in 70% ammonium sulfate suspension containing 2 mM DTT at 4°C. Mutations of $F_oF_1$ were introduced into the plasmid pTR-T$F_oF_1$-ASDS-εΔc in which $F_1$-coding region is the same as pKAGB1/HC95 and the C-terminal domain of the ε subunit is deleted (26). $F_oF_1$ was expressed and purified as described (27,28). The purified $F_oF_1$ preparation was frozen by liquid $N_2$, and stored at -80°C until use. The yields of purified mutant $F_1$s and $F_oF_1$s were 20 - 50 % of that of the wild-type. The purity of the isolated preparations, exemplified by the three mutants that are the main focus of this paper, is shown (Fig. S1). The concentrations of $F_1$ and $F_oF_1$ were determined from the absorbance with the molar extinction coefficient at 280 nm of 154,000 $M^{-1}cm^{-1}$ and 253,000 $M^{-1}cm^{-1}$ and with the molecular weight as 356 kDa and as 530 kDa, respectively (25,29).

*Observation and analysis of rotation* ---- Rotation was observed on the stage of an inverted microscope (IX70, Olympus) at 25°C as described (21). A mercury lamp was used to observe rotation of 209 nm, 291 nm, and 350 nm polystyrene beads, and a 532-nm laser to observe rotation of 40-nm gold beads. Images of beads were captured with a CCD camera (ICL-B0620M-KC, IMPERX and GX-8, nac) with 250 frames per sec (fps) for polystyrene beads and with 4,000 fps for gold beads. The glass chamber was made of the Ni-NTA-coated bottom coverslip (21) and an uncoated top coverslip. The bottom coverslip and the top coverslip were separated by two strips of double-faced tape. $F_1$ was biotinylated by incubation with biotin-PEAC5-maleimide for 90 min. The biotinylated $F_1$ (10 nM) in 50 mM MOPS/KOH, pH7.0, containing 50 mM KCl and 10 mg/ml bovine serum albumin was applied into the chamber and overflowing solution was blot with paper. After 2 min, the chamber was washed by 50 mM MOPS/KOH containing 50 mM KCl, and beads suspended in 50 mM MOPS/KOH, 50 mM KCl, and 10 mg/ml bovine serum albumin were applied into the chamber. After waiting for 15 min and washing, the rotation buffer (50 mM MOPS/KOH pH7.0, 50 mM KCl, 2 mM $MgCl_2$, 1 mM phosphoenolpyruvate (SIGMA), 200 μg/ml pyruvate kinase (Roche), and indicated concentration of ATP) was applied into the chamber. As commonly experienced for single molecule observations of this kind, only a few percent, at most, of beads showed clear rotation due to surface denaturation, improper bead attachment and other unknown reasons. Numbers of rotating beads of mutant $F_1$ molecules were slightly fewer than that of wild-type $F_1$. Rotating beads rotated at various speeds. In general fast rotating beads always rotated quickly, whereas sluggish ones almost never showed fast rotation. The rotations at the fastest speed were analyzed, because slower rotation can be explained by surface obstructions.

Torque of rotation was defined as

$$N=\omega\xi$$

where ω and ξ are the rotation speed (radian/sec) and viscous load, respectively. The value of ξ of

duplex beads is given as

$$\xi=16\pi\eta r^3+6\pi\eta r x_1^2+6\pi\eta r x_2^2$$

where $\eta$ is the viscosity of a medium ($\eta=0.93\times10^{-9}$ pN/nm$^2$), r and $x_i$ (i = 1, 2) are the radius and rotation radius of each bead, respectively (30). The beads rotating with about the same rotation radius were selected and analyzed. Torque was also estimated from fluctuation analysis (31) and defined as

$$\ln[P(\Delta\theta)/P(-\Delta\theta)] = N\Delta\theta/k_BT$$

where N is torque, $k_B$ is the Boltzmann constant, T is temperature (T=298K), $\Delta\theta=\theta(t+\Delta t)-\theta(t)$, $\Delta t$ is 4 msec, and $P(\Delta\theta)$ is the probability distribution of $\Delta\theta$. One can estimate N from this equation without the value of $\xi$.

*ATP-driven proton pumping and ATP synthesis* ---- Purified $F_oF_1$ was reconstituted into proteoliposomes by using BioBeads as described (28). Proteoliposome suspension (20 μl) was mixed with 1.2 ml of 10 mM HEPES/KOH, pH7.5, 5 mM $MgCl_2$, 100 mM KCl, and 0.3 μg/ml 9-amino-6-chloro-2-methoxyacridine (ACMA). The reaction was started by addition of 12 μl of 100 mM ATP, and formation of a transmembrane pH gradient ($\Delta$pH) was monitored with quenching of ACMA fluorescence (excitation 410 nm, emission 480 nm) at 25°C. Final concentrations of $F_oF_1$ were 11.4 nM. At the end of measurement, nigericin (2 μM) was added to eliminate $\Delta$pH. ATP synthesis was measured as described (27) except for a long (6 hr) incubation of proteoliposome with the acidic mixture (35 mM MES, 10 mM $NaH_2PO_4$, 2.5 mM $MgCl_2$, 0.68 mM KCl, 340 mM sucrose, 0.5 mM ADP, 0.2 μM valinomycin, pH6.05). A basic mixture was prepared by mixing 21 μl of the luciferin/luciferase mixture (2×concentration, ATP bioluminescence assay kit CLSII, Roche), 870 μl of the basic buffer (300 mM HEPES, 10 mM $NaH_2PO_4$, 2.5 mM $MgCl_2$, 240 mM KOH, pH adjusted with NaOH to 8.05) and 9 μl of 50 mM ADP, and was incubated for 5 min at 30°C. The acidic mixture containing proteoliposome (100 μl) was added into 900 μl of the basic mixture and emission of luciferin was monitored. Calculated size of the imposed pmf was 260 mV ($\Delta$pH=2, $\Delta\psi$=140 mV). Final concentration of $F_oF_1$, ADP and $P_i$ were 11.4 nM, 0.5 mM, and 10 mM, respectively. Final pH of the solution outside the proteoliposomes was 8.05. At the end of measurements, 10 μl of 10 μM ATP was added three times for calibration (28).

## RESULTS

*Torque mutants of $F_1$* ---- $F_1$ with decreased torque is expected to rotate beads slowly compared with the wild-type $F_1$. For the search for structural features responsible for the torque generation, various mutants of *Bacillus* PS3 $F_1$ were expressed in *E. coli*. They are, in most cases, expressed in smaller amount and are less heat-stable than the wild-type but purified without difficulty. The purified $F_1$ was immobilized onto the Ni-NTA coated glass surface through His-tagged β subunits and 291 nm polystyrene beads were attached on the γ subunit as a rotation probe. We observed the rotation of duplex beads in 2 mM ATP under the microscopic field with a camera (250 fps). Under these experimental conditions, ATP-waiting dwell and catalytic dwell are too short to be observed and continuous rotations with occasional pauses by ADP-Mg inhibition or for other reasons were observed. Among beads rotating at various speeds, the rotations at the fastest speed were taken to be the unobstructed rotation of native molecules.

We at first focused on amino acid residues that are located at the rotor/stator interface narrower than 3.5 Å at the orifice region. Except for the residues in the $^{390}$DELSDED$^{396}$ sequence of the β subunit that were already demonstrated not to be critical for torque generation, we replaced these residues with alanine and made $F_1$ variants containing mutations αG398A/S399A/D400A, αD400A/L401A/D402A, γD83A/R84A/G85A, γG85A/L86A, γG88A, γY90A/N91A or γN91A/S92A/N93A. We found that these mutants rotated beads at speeds similar to the wild-type $F_1$, ~20 revolution per sec (rps) (data

not shown), indicating that specific interactions between side chains of these residues do not significantly contribute to torque generation. Next, we made two mutant $F_1$s, $\beta\Delta^{388}$GMDE$^{391}$ and $\beta\Delta^{392}$LSD$^{394}$, that have a deletion in the $^{388}$GMDELSDED$^{396}$ sequence of β subunit (Fig. 1, right panel), but again they showed rotation at a normal speed (Fig. 2, upper panels). Then, we deleted one or two turns of the helix-1 that precedes the $^{390}$DELSDED$^{396}$ sequence and $\beta\Delta^{380}$LQDI$^{383}$, $\beta\Delta^{376}$RYKE$^{379}$ and $\beta\Delta^{377}$YKELQDI$^{383}$ were made (Fig. 1, right panel) (superscripts are abbreviated hereafter). These three mutant $F_1$s rotated more slowly than the wild-type $F_1$ (Fig. 2, lower panels) and we focused on these mutants.

*Half-torque $F_1$* ---- Torque of the three mutants relative to that of wild-type $F_1$ was estimated from three different analyses. First, continuous rotation of 209 nm, 291 nm and 350 nm duplex beads in 2 mM ATP was analyzed. The rotation speed of each mutant $F_1$ was obtained from the consecutive, smooth 10 revolutions taken from the five fastest-rotating molecules. As the size of bead increases, viscous load increases and rotation slows down (Fig. 3A). With beads of the same size, viscous load is constant and torque is obtained from the equation (torque =viscous load x rotation speed) (Fig. 3B). The averaged torque with three different sizes of beads is 46 pN·nm (wild-type), 29 pN·nm (βΔRYKE), 26 pN·nm (βΔLQDI), and 22 pN·nm (βΔYKELQDI). Second, rotation of 291 nm duplex beads in 200 nM ATP was observed. At this low ATP concentration, $F_1$ repeats a pause of ATP-waiting dwell and a 120°-step rotation. The consecutive ten 120°-step rotations were overlaid and averaged (Fig. 3C). Torque was estimated from the rotation speed of the middle part of the averaged 120°-step rotation trajectory. As seen (Fig. 3D), torques of mutants obtained by this analysis are slightly larger than those obtained from continuous rotation. Third, bead fluctuation during rotational motion was analyzed by the recently developed fluctuation theorem (Fig. 3E). By this analysis, the magnitude of torque is directly obtained from fluctuation of rotating beads without knowledge of the values of viscous load and rotation speed. This is advantageous because the estimation of viscous load needs information of exact size of individual beads, rotational radius, and viscosity of the medium near the surface of glass and may contain errors (32). The averaged torque with three different sizes of beads is 47 pN·nm (wild-type), 22 pN·nm (βΔRYKE), 23 pN·nm (βΔLQDI), and 22 pN·nm (βΔYKELQDI). Altogether, three independent methods give similar torque values for all three mutant $F_1$s, that is, about half of the normal torques of wild-type $F_1$. Thus, shortening of the helix-1 results in the loss of half of the torque. Out of the energy supplied by hydrolysis of one ATP molecule for 120°-rotation, these mutant $F_1$s can utilize only ~45 pN·nm (= torque x $2\pi/3$) while wild-type $F_1$ can utilize ~90 pN·nm.

*Kinetic constants of half-torque $F_1$s* ---- Kinetic characteristics of half-torque $F_1$, termed $F_{1(1/2)}$ hereafter, were examined by analysis of rotation. First, durations of ATP-waiting dwell in rotation in 200 nM ATP were collected and plotted as histograms (Fig. 4A). The histograms are fitted by an exponential function that contains the rate of ATP binding ($k_{on}$) to the catalytic site. The $k_{on}$ values that give the best fit are 2.0 x $10^7$ $M^{-1}s^{-1}$ (wild-type), 1.6 x $10^7$ $M^{-1}s^{-1}$ (βΔRYKE), 0.7 x $10^7$ $M^{-1}s^{-1}$ (βΔLQDI) and 1.3 x $10^7$ $M^{-1}s^{-1}$ (βΔYKELQDI). Taking into account that the values of βΔLQDI and βΔYKELQDI might be underestimated because fitting curves are dragged to the right by the presence of dwells longer than 2 sec of unknown origin, it appears that $k_{on}$ values of $F_{1(1/2)}$s are not significantly changed from that of wild-type $F_1$.

Next, rotation of a 40-nm single gold bead attached to γ subunit was observed in 2 mM ATP with a high speed camera (4,000 fps). Under these conditions, viscous load of bead rotation is negligible, ATP-waiting dwell is not observed, and only catalytic dwell is observed at each 120° interval. The histogram of durations

of the catalytic dwells is fitted by a double exponential function defined by two time constants (Fig. 4B). Previous studies assigned two time constants to the two sequential catalytic events on the enzyme, ATP hydrolysis and $P_i$ release (16). Two of the $F_{1(1/2)}$s have time constants (βΔRYKE, 0.5 ms and 1.2 ms; βΔYKELQD, 0.5 ms and 1.1 ms), which are very similar to those of the wild-type $F_1$ (0.4 ms and 1.4 ms). The βΔLQDI mutant has slightly longer time constants (0.8 ms and 1.3 ms). Enzyme turnover rates calculated from the above values are 560 $s^{-1}$ (wild-type), 590 $s^{-1}$ (βΔRYKE), 480 $s^{-1}$ (βΔLQDI), 630 $s^{-1}$ (βΔYKELQDI). ATP hydrolysis activities measured in the bulk solution containing 2 mM ATP are 330 $s^{-1}$ (wild-type), 270 $s^{-1}$ (βΔRYKE), 110 $s^{-1}$ (βΔLQDI), and 330 $s^{-1}$ (βΔYKELQDI) in the presence of lauryldimethyamine-N-oxide, which is thought to relieve ADP-Mg inhibition. Taking into account that purified $F_1$s may contain some fraction of inactive molecules, these values are compatible with values obtained from rotation. To summarize the above results, enzyme kinetics of $F_{1(1/2)}$s are not changed much from those of wild-type $F_1$.

*Proton pumping and ATP synthesis* ---- *Bacillus* PS3 $F_oF_1$ containing $F_{1(1/2)}$ was expressed in *E. coli* and purified. The purified mutant $F_oF_1$s are as stable as the wild-type. To avoid complexity caused by regulatory function of the ε subunit, the C-terminal domain of the ε subunit (εΔC) was deleted and will be termed wild-type $F_oF_1$ hereafter (26,33,34). The purified $F_oF_1$ was reconstituted into proteoliposomes and ATP-driven proton pumping was monitored with the quenching of ACMA fluorescence that reflects pH gradient across membranes (ΔpH). Upon addition of ATP, quenching started with a short lag, progressed at a maximum rate, and leveled off at the stationary phase (Fig. 5A). The established ΔpH was completely abolished by the addition of nigericin, a $H^+$-$K^+$ antiporter which can dissipate ΔpH. In general, quenching time courses of the three $F_oF_{1(1/2)}$s are very similar to each other. The fastest quenching progress rates of $F_oF_{1(1/2)}$s are about 40 % of that of wild-type $F_oF_1$ and the maximum quenching level at the stationary phase with $F_oF_{1(1/2)}$s was ~60 % of that of wild-type $F_oF_1$. Thus, $F_oF_{1(1/2)}$s can pump protons but the final ΔpH built up is much smaller than that of wild-type $F_oF_1$.

Using the same proteoliposomes, we observed ATP synthesis driven by acid-base transition and valinomycine-induced $K^+$-diffusion potential (Fig. 5B). The reaction was started by addition of acidified proteoliposome mixture into the basic mixture and generation of ATP was monitored by luciferin/luciferase. In the presence of nigericin, which acts as an uncoupler in combination with valinomycin, ATP synthesis did not occur. In contrast to proton-pumping, activities of ATP synthesis of the $F_oF_{1(1/2)}$s are different from each other and initial rates of synthesis are 28 % (βΔRYKE), 20 % (βΔLQDI) and 11 % (βΔYKELQDI) of that of wild-type $F_oF_1$.

## DISCUSSION

*Short-sized helix-1 impairs energy conversion but not chemical catalysis* ---- Properties of the half-torque mutants are summarized in Table 1. As seen, when the mutant enzymes hydrolyze ATP without the burden of the viscous load, their enzymatic kinetics are not very different from those of the wild-type enzyme. However, once they have to do work such as rotating large beads and pumping protons, their defect become obvious. Thus, shortening of helix-1 does not impair chemical catalysis but does impair mechnochemical energy conversion.

*Torque generation in $F_{1(1/2)}$* ---- The half-torque mutants we reported here retain the sleeve interactions. In addition, they do not lose all orifice interactions but retain the interactions at the conical entrance of the orifice of $\alpha_3\beta_3$-ring that touches the globular portion of the γ subunit (Fig. 1). $F_1$ with the truncated γ subunit, which apparently has only the interactions with the conical entrance region of the $\alpha_3\beta_3$-ring, can generate a small torque that barely supports

unidirectional slow rotation of a load-negligible gold bead (35). It appears, therefore, that the sleeve interactions coordinated with the interactions at the conical entrance would be responsible for the generation of torque in $F_{1(1/2)}$s.

*Helix-1 with sufficient length is necessary for torque generation, acting as pushrod* ---- The orifice interactions by themselves produce at least half of the torque of the ATP-driven $F_1$-motor (21,35). Given that the interactions at the conical entrance region contribute only a small fraction of the torque, the majority of the torque produced at the orifice is attributed to the interactions of the helix-1−loop−helix-2 with the convex coiled-coil region of the γ subunit. Concerning the central loop, the conserved DELSDEAD sequence is not necessary for the torque generation (23). Even the mutants with the shortened loop can synthesize ATP (24) and produce normal torque (Fig. 2). Instead, this work reveals a critical role of full-length helix-1 in the generation of torque. When helix-1 is shortened by one helical turn (5.4Å) by deletion of either the RYKE or LQDI segments, torque is reduced by half. When the segment RYKELQDI, which forms two turns (10.8Å) in helix-1, is truncated, torque is again reduced by no more than half. It is clear from these results that the physical length, rather than residue-specific interactions, of helix-1 is important for torque generation. In addition, the fact that deletion of one turn and of two turns gives the same result implies the presence of a critical length for helix-1 function. Crystal structure (36), single molecule study (37) and rapid scan AFM (38) show that C-terminal domains of three β subunits in $F_1$ undergo bending motion sequentially and alternately during catalytic cycle. The helix-1−loop−helix-2 is a protruding body of the C-terminal domain toward the γ subunit (Fig. 1) and it can protrude more toward the γ subunit by a bending motion (36). It appears that a protruding solid body of the helix-1−loop−helix-2 physically pushes the convex part of the coiled-coil of the γ subunit and assists the γ subunit to rotate (39). To transmit the force, helix-1, and probably helix-2 as well, must play the role of "pushrod" with sufficient length and stiffness.

*On the critical length of the helix-1* ---- Very recently, more research on the helix-1−loop−helix-2 structure was published by Mnatsakanyan *et al* (40). They found that a mutant of *Bacillus* PS3 $F_oF_1$, Δ7 (βΔ(LQDI+LSD)), can catalyze ATP synthesis, though slowly, but Δ10 (βΔ(QDIIAIL+LSD)) cannot. From the difference between Δ7 and Δ10, Mnatsakanyan *et al* concluded that the critical length of the helix-1−loop−helix-2 structure is around ~10Å shorter than the native length. Our results clearly show that shortening one turn (~5Å) of helix-1 (βΔLQDI and βΔRYKE) is enough to abolish half of the torque. Therefore, we agree on the presence of a critical length, but propose that critical length of the helix as a solid body is ~5Å shorter than the native length. Most likely, Δ10 is also a half-torque mutant and has catalytic ability of ATP synthesis, though it might have been very weak and escaped the assay employed in (40). Actually, Δ10 retains proton-pumping activity, though weak (40), which should not happen without torque.

*Low-torque $F_oF_1$ builds up a small ΔpH* ---- Given that $F_{1(1/2)}$ can use only a fraction of the energy of ATP hydrolysis for driving the motor, it is reasonable to assume that $F_oF_{1(1/2)}$ can also use only a fraction of the energy for proton-pumping. Indeed, the final ΔpH built up by the proton-pumping action of $F_oF_{1(1/2)}$ is significantly smaller than ΔpH built up by wild-type $F_oF_1$. Final ΔpH could be determined by equilibrium between proton-pumping activity and back pressure of pmf and/or equilibrium between proton-pumping activity and passive leakage of protons through membranes. In any case, however, the fact that three kinds of $F_oF_{1(1/2)}$s build up the same final ΔpH indicates that final ΔpH is directly determined by the magnitude of the torque, that is, by the energy conversion yield. It agrees with the thermodynamic prediction that ΔpH is directly

related to the torque (n x ZΔpH = torque x 2π/3; where n is the number of transported protons per ATP, and Z is a constant).

*Low-torque $F_oF_1$ can synthesize ATP slowly under thermodynamically favorable conditions* ---- If the same inefficient energy conversion occurs in the ATP synthesis reaction of $F_oF_{1(1/2)}$, the $F_{1(1/2)}$ portion of $F_oF_{1(1/2)}$ can use only a fraction (~45 pN·nm per 120° rotation) of the total energy provided by $F_o$ portion. Despite this defect, $F_oF_{1(1/2)}$ can synthesize ATP (Fig. 5B). This might be owing to the small free energy required for ATP synthesis under actual experimental conditions. The reaction mixtures contained 0.5 mM ADP and 10 mM $P_i$. The ADP we used contained about 0.05 % ATP as measured by luciferase assay and the free energy required for ATP synthesis would amount to ~40 pN·nm, which the $F_{1(1/2)}$ portion of $F_oF_{1(1/2)}$ can manage to exert. Therefore, low-torque $F_oF_1$ has catalytic ability and can synthesize ATP under optimum thermodynamic situations.

Since the free energy defines the direction and equilibrium but not the rate of the reaction, it is not surprising that each of the three $F_oF_{1(1/2)}$s catalyzes ATP synthesis at a different rate. Subtle variations in the enzyme can affect the rate, and the reason for the slow ATP synthesis rate of $F_oF_{1(1/2)}$s cannot be explained with certainty. During the ATP synthesis reaction, the $F_o$ portion provides energy to the $F_1$ portion via rotation of the γ subunit. The $F_1$ portion uses this energy to induce the otherwise thermodynamically unfavorable conformational changes to β subunits that lead to ATP synthesis. We speculate that, with insufficient ability to utilize energy, $F_oF_{1(1/2)}$ would fail frequently and take a long time to induce such changes, or even make uncoupled rotations frequently without inducing such changes. We observed that the $F_oF_{1(1/2)}$s have larger uncoupled ATP hydrolysis activity than wild-type $F_oF_1$, which is probed by resistance to inactivation by dicyclohexylcarbodiimide, a reagent that prevents proton translocation and hence rotation of $F_o$. This observation favors the scenario of the uncoupled rotation but does not exclude other interpretations.

Finally, it should be noted that even though $F_oF_{1(1/2)}$ can synthesize ATP, the synthesis reaction reaches equilibrium when ATP concentration is four or five orders of magnitude lower than in the case of wild-type $F_oF_1$. This means that cellular ATP concentration supported by $F_oF_{1(1/2)}$ would be very low and could hardly sustain normal cell activities. Thus, natural selection would not allow field organisms to have a low-torque version of $F_oF_1$, even if it had catalytic ability of ATP synthesis.



REFERENCES


1. Yoshida, M., Muneyuki, E., and Hisabori, T. (2001) *Nat Rev Mol Cell Biol* **2**, 669-677
2. Boyer, P. D. (2002) *J Biol Chem* **277**, 39045-39061
3. Senior, A. E., Nadanaciva, S., and Weber, J. (2002) *Biochim Biophys Acta* **1553**, 188-211
4. Kinosita, K., Jr., Adachi, K., and Itoh, H. (2004) *Annu Rev Biophys Biomol Struct* **33**, 245-268
5. Weber, J. (2006) *Biochim Biophys Acta* **1757**, 1162-1170
6. Nakamoto, R. K., Baylis Scanlon, J. A., and Al-Shawi, M. K. (2008) *Arch Biochem Biophys* **476**, 43-50
7. Junge, W., Sielaff, H., and Engelbrecht, S. (2009) *Nature* **459**, 364-370
8. Duser, M. G., Zarrabi, N., Cipriano, D. J., Ernst, S., Glick, G. D., Dunn, S. D., and Borsch, M. (2009) *Embo J* **28**, 2689-2696
9. von Ballmoos, C., Wiedenmann, A., and Dimroth, P. (2009) *Annu Rev Biochem* **78**, 649-672

10. Nakanishi-Matsui, M., Sekiya, M., Nakamoto, R. K., and Futai, M. (2010) *Biochim Biophys Acta* **1797**, 1343-1352
11. Noji, H., Yasuda, R., Yoshida, M., and Kinosita, K., Jr. (1997) *Nature* **386**, 299-302
12. Itoh, H., Takahashi, A., Adachi, K., Noji, H., Yasuda, R., Yoshida, M., and Kinosita, K. (2004) *Nature* **427**, 465-468
13. Rondelez, Y., Tresset, G., Nakashima, T., Kato-Yamada, Y., Fujita, H., Takeuchi, S., and Noji, H. (2005) *Nature* **433**, 773-777
14. Yasuda, R., Noji, H., Yoshida, M., Kinosita, K., Jr., and Itoh, H. (2001) *Nature* **410**, 898-904
15. Shimabukuro, K., Yasuda, R., Muneyuki, E., Hara, K. Y., Kinosita, K., Jr., and Yoshida, M. (2003) *Proc Natl Acad Sci U S A* **100**, 14731-14736
16. Adachi, K., Oiwa, K., Nishizaka, T., Furuike, S., Noji, H., Itoh, H., Yoshida, M., and Kinosita, K., Jr. (2007) *Cell* **130**, 309-321
17. Yasuda, R., Noji, H., Kinosita, K., Jr., and Yoshida, M. (1998) *Cell* **93**, 1117-1124
18. Ariga, T., Muneyuki, E., and Yoshida, M. (2007) *Nat Struct Mol Biol* **14**, 841-846
19. Abrahams, J. P., Leslie, A. G., Lutter, R., and Walker, J. E. (1994) *Nature* **370**, 621-628
20. Bowler, M. W., Montgomery, M. G., Leslie, A. G., and Walker, J. E. (2007) *J Biol Chem* **282**, 14238-14242
21. Hossain, M. D., Furuike, S., Maki, Y., Adachi, K., Suzuki, T., Kohori, A., Itoh, H., Yoshida, M., and Kinosita, K., Jr. (2008) *Biophys J* **95**, 4837-4844
22. Kohori, A., Chiwata, R., Hossain, M. D., Furuike, S., Shiroguchi, K., Adachi, K., Yoshida, M., and Kinosita, K., Jr. (2011) *Biophys J* **101**, 188-195
23. Hara, K. Y., Noji, H., Bald, D., Yasuda, R., Kinosita, K., Jr., and Yoshida, M. (2000) *J Biol Chem* **275**, 14260-14263
24. Mnatsakanyan, N., Krishnakumar, A. M., Suzuki, T., and Weber, J. (2009) *J Biol Chem* **284**, 11336-11345
25. Suzuki, T., Ueno, H., Mitome, N., Suzuki, J., and Yoshida, M. (2002) *J Biol Chem* **277**, 13281-13285
26. Konno, H., Suzuki, T., Bald, D., Yoshida, M., and Hisabori, T. (2004) *Biochem Biophys Res Commun* **318**, 17-24
27. Suzuki, T., Murakami, T., Iino, R., Suzuki, J., Ono, S., Shirakihara, Y., and Yoshida, M. (2003) *J Biol Chem* **278**, 46840-46846
28. Soga, N., Kinosita, K., Jr., Yoshida, M., and Suzuki, T. (2011) *Febs J* **278**, 2647-2654
29. Furuike, S., Adachi, K., Sakaki, N., Shimo-Kon, R., Itoh, H., Muneyuki, E., Yoshida, M., and Kinosita, K., Jr. (2008) *Biophys J* **95**, 761-770
30. Sakaki, N., Shimo-Kon, R., Adachi, K., Itoh, H., Furuike, S., Muneyuki, E., Yoshida, M., and Kinosita, K., Jr. (2005) *Biophys J* **88**, 2047-2056
31. Hayashi, K., Ueno, H., Iino, R., and Noji, H. (2010) *Phys Rev Lett* **104**, 218103
32. Panke, O., Cherepanov, D. A., Gumbiowski, K., Engelbrecht, S., and Junge, W. (2001) *Biophys J* **81**, 1220-1233
33. Feniouk, B. A., Suzuki, T., and Yoshida, M. (2007) *J Biol Chem* **282**, 764-772
34. Masaike, T., Suzuki, T., Tsunoda, S. P., Konno, H., and Yoshida, M. (2006) *Biochem Biophys Res Commun* **342**, 800-807
35. Furuike, S., Hossain, M. D., Maki, Y., Adachi, K., Suzuki, T., Kohori, A., Itoh, H., Yoshida, M., and Kinosita, K., Jr. (2008) *Science* **319**, 955-958
36. Bowler, M. W., Montgomery, M. G., Leslie, A. G., and Walker, J. E. (2006) *Proc Natl Acad Sci U S A* **103**, 8646-8649
37. Masaike, T., Koyama-Horibe, F., Oiwa, K., Yoshida, M., and Nishizaka, T. (2008) *Nat Struct Mol Biol* **15**, 1326-1333
38. Uchihashi, T., Iino, R., Ando, T., and Noji, H. (2011) *Science* **333**, 755-758

39. Oster, G., and Wang, H. (2003) *Trends Cell Biol* **13**, 114-121
40. Mnatsakanyan, N., Kemboi, S.K., Salas, J., and Weber, J. (2011) *J Biol Chem* **286**, 29788-29796

Acknowledgement --- We thank Mr. Daniel Xu for critically reading and polishing English.

FOOTNOTES

*This work was supported by the ATP synthesis Regulation Project (ICORP) organized for M. Yoshida by Japan Science and Technology Agency.

[1] The abbreviation used are: fps, frames per sec; ACMA, 9-amino-6-chloro- 2-methoxyacridine; $F_{1(1/2)}$, mutant $F_1$ that rotates with half torque of the wild-type $F_1$; pmf, proton motive force; rps, revolution per sec

FIGURE LEGENDS

Fig.1. Structure around the DELSDED loop
Left panel. Structure of α, β and γ subunits in bovine $F_1$ (PDB ID: 2v7q). Orifice and sleeve regions, and N- and C-termini of γ subunit are indicated. The region corresponding to the helix-1, DELSDED loop, and helix-2 of the β subunit are shown in red. Right panel. helix-1−DELSDED loop−helix-2 region of β subunit of *Bacillus* PS3 $F_1$. Sequences truncated in this work are shown by blue lines (upper panel) and blue stretches (lower panel).

Fig. 2. Rotation trajectories of rotating duplex beads in 2 mM ATP. Bead size is 291 nm. Each line represents rotation of each $F_1$ molecule. Experimental details are described in EXPERIMENTAL PROCEDURES.

Fig. 3. Torque measurement by three methods. A. Continuous rotation of three different beads in 2 mM ATP. For each size bead, ten consecutive, smooth revolutions were selected from the five fastest rotation trajectories out of several tens of observed rotations and time-averaged slope of the trajectory was obtained as rotation speed (shown by circle). The average of five circles is shown by a square symbol. Wild-type $F_1$ is shown in red, and mutants, blue. Viscous load was calculated from bead size, rotation radius and viscous coefficient. The lines of constant torque (50, 40, 30, 20 pN·nm from the top) are shown. B. Torques calculated from A. Labels of bars are wild-type, βΔRYKE, βΔLQDI and βΔYKELQDI from the top as in D. C. 120°-step rotation of 291 nm beads in 200 nM ATP. Ten consecutive 120°-step rotations were overlaid, averaged (blue, thick line) and then the slope between 30° and 90° (red line) was obtained as rotation speed. D. Torques obtained from C. E. Fluctuation analysis of rotation of three differently beads in 2 mM ATP. Δθ is the difference between rotary angles after 4 ms. P(Δθ) is a distribution function of Δθ. Wild-type $F_1$, red; mutant $F_1$, blue. F. Torques obtained from E. Labels of bars are the same as D. Experimental details are described in EXPERIMENTAL PROCEDURES.

Fig. 4. Kinetic constants of $F_{1(1/2)}$s. A. Histogram of ATP-waiting dwell of rotation of 291 nm duplex beads in 200 nM ATP recorded by 250 fps. ATP binding rate constant ($k_{on}$) is obtained from a fitting curve (solid line), constant×exp(-$k_{on}$×[ATP]×t). B. Histogram of catalytic dwell of rotation of a 40-nm gold bead in 2 mM ATP recorded by 4,000 fps. The data is fitted by a double exponential function (solid line), constant×(exp(-(1/$\tau_1$)×t) – exp(-(1/$\tau_2$)×t). $\tau_1$ and $\tau_2$ represent the time constants of two successive reactions, ATP hydrolysis and $P_i$ release, that occur in the catalytic dwell (16). Experimental details are described in EXPERIMENTAL PROCEDURES.

Fig. 5. Activities of $F_oF_{1(1/2)}$s. A. ATP-driven proton-pump. Acidification of the inside lumen of $F_oF_{1(1/2)}$-containing proteoliposomes by proton pumping was monitored with fluorescence quenching of ACMA. The reaction was started by addition of 1 mM ATP. B. ATP synthesis activity. The $F_oF_{1(1/2)}$-containing proteoliposomes were pre-equilibrated with the low $K^+$, acidic mixture and then injected into a ten-fold volume of the high $K^+$ basic mixture. Acidic mixture contained ADP, $P_i$ and valinomycin. Basic mixture contained ADP, $P_i$ and luciferin/luciferase. Final concentration of $F_oF_1$, ADP and $P_i$ were 11.4 nM, 0.5 mM, and 10 mM, respectively. ATP produced was monitored with emission of luciferin and the initial slope of exponential fitting curve between 0-6 sec was taken to be ATP synthesis activity as shown in the right side of figure. Experimental details are described in EXPERIMENTAL PROCEDURES.

Table 1. Properties of mutant $F_1$s and $F_oF_1$s with short-sized pushrod helix

| | $F_1$ | | | $F_oF_1$ | |
|---|---|---|---|---|---|
| mutants | torque[*1] | $k_{on(ATP)}$ | catalytic events[*2] | $H^+$-pump[*3] | ATP synthesis |
| | *pN·nm* | $\times 10^7 M^{-1}s^{-1}$ | *τ (ms)* | *ΔF (%)* | $s^{-1}$ |
| wild-type | 46, 50, 47 | 2.0 | 0.37, 1.1 | 64 | 8.8 ± 0.8 |
| βΔRYKE | 29, 34, 22 | 1.6 | 0.48, 1.2 | 38 | 2.5 ± 0.4 |
| βΔLQDI | 26, 29, 23 | 0.7 | 0.81, 1.4 | 40 | 1.8 ± 0.1 |
| βΔYKELQDI | 22, 29, 22 | 1.3 | 0.46, 1.1 | 43 | 1.0 ± 0.2 |

*[1] Torque values (from left) from Fig. 3B, 3D, and 3F.
*[2] Life times of two catalytic events (ATP cleavage and Pi release) that occur on the enzyme at the catalytic dwell (from Fig. 4).
*[3] Typical values of ACMA fluorescence quenching (Fig. 5).

Fig. 1. Usukura et al

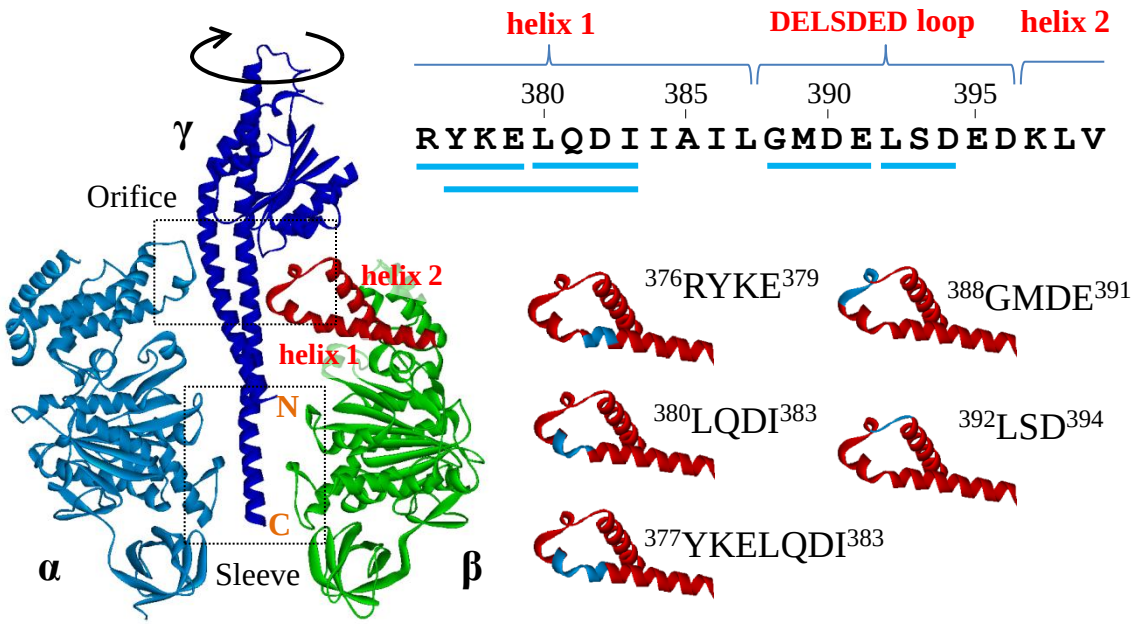

Fig. 2. Usukura et al

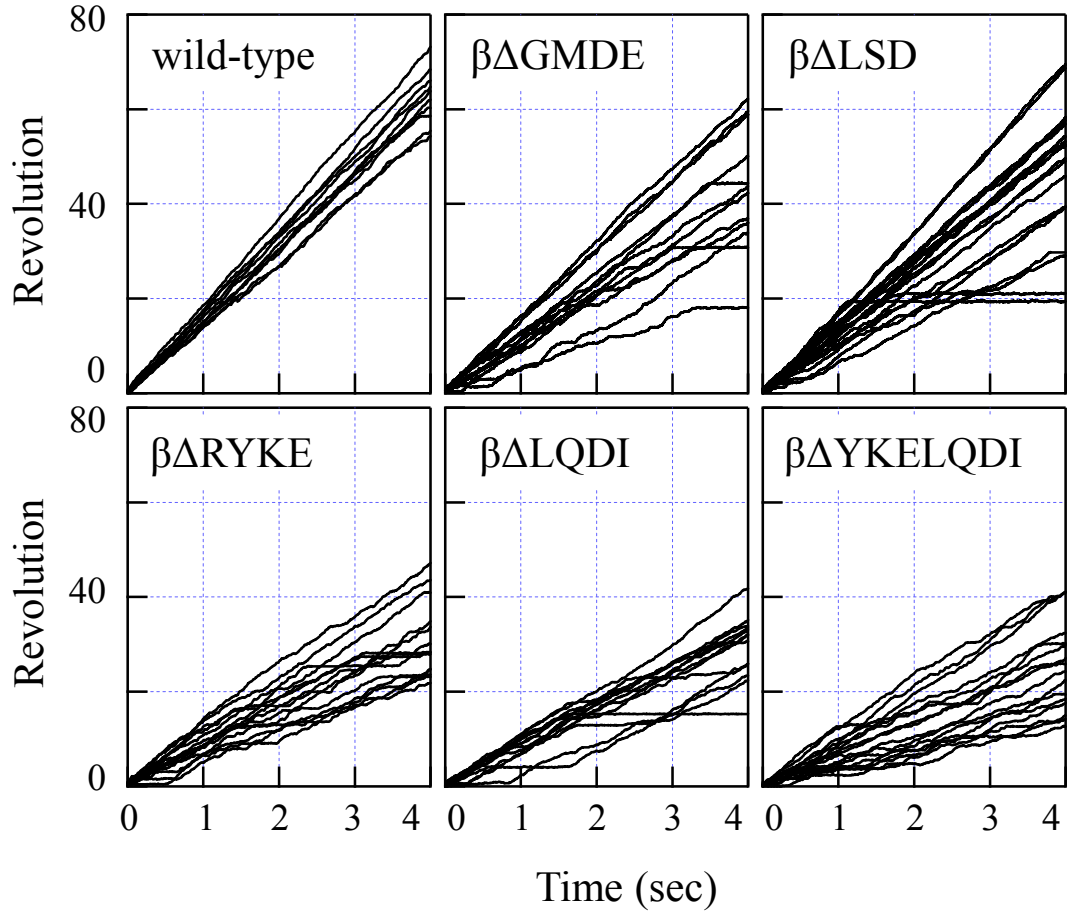

Fig. 3. Usukura et al

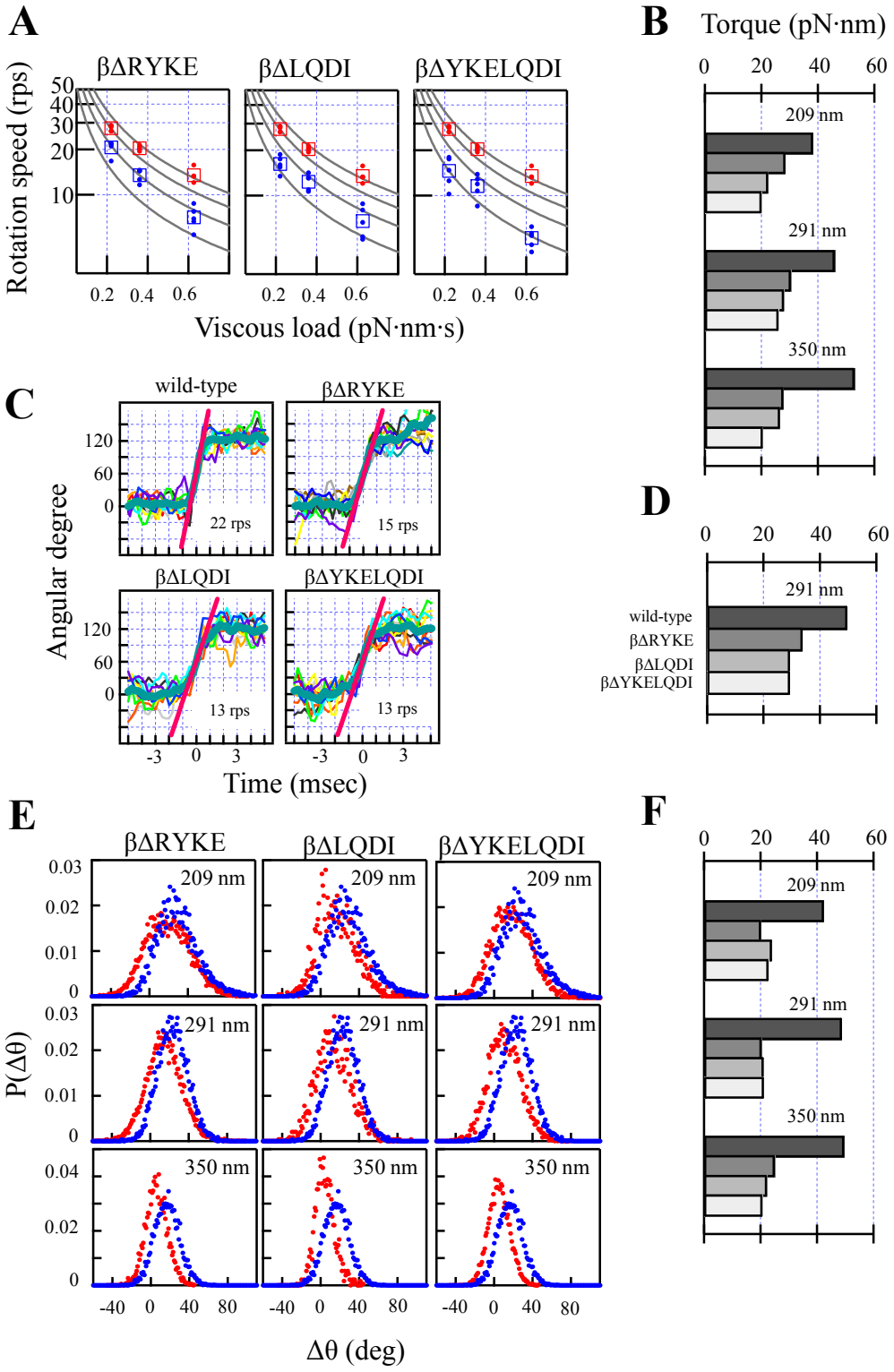

Fig. 4. Usukura et al

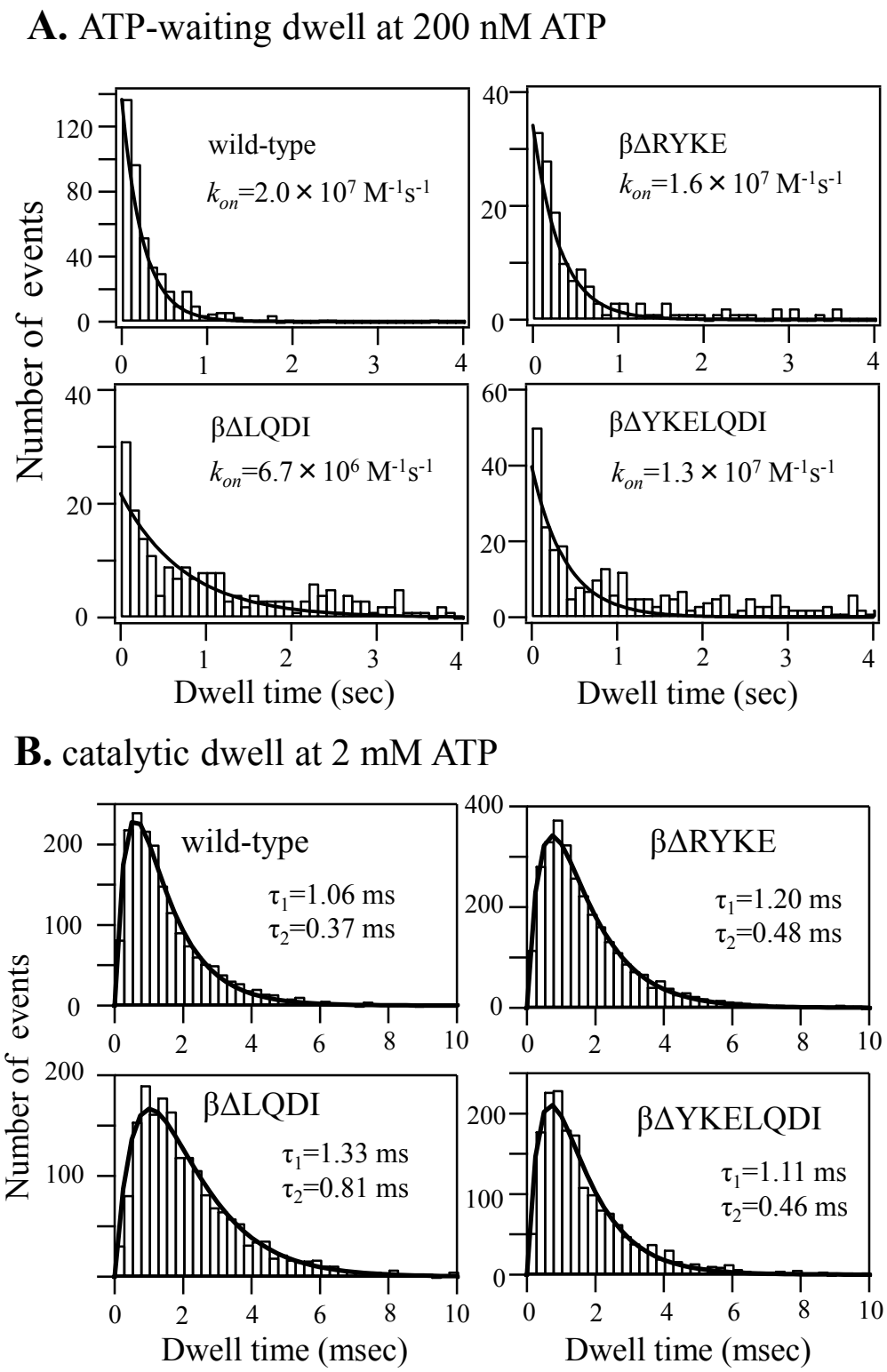

Fig. 5. Usukura et al